

TECHNICAL RESEARCH REPORT

Computational Micromagnetics for Magnetostrictive Actuators

by X. Tan, J.S. Baras, P.S. Krishnaprasad

CDCSS T.R. 2000-5
(ISR T.R. 2000-18)



The Center for Dynamics and Control of Smart Structures (CDCSS) is a joint Harvard University, Boston University, University of Maryland center, supported by the Army Research Office under the ODDR&E MURI97 Program Grant No. DAAG55-97-1-0114 (through Harvard University). This document is a technical report in the CDCSS series originating at the University of Maryland.

Web site <http://www.isr.umd.edu/CDCSS/cdcss.html>

Computational micromagnetics for magnetostrictive actuators*

Xiaobo Tan, John S. Baras, and P. S. Krishnaprasad

Institute for Systems Research and
Department of Electrical and Computer Engineering
University of Maryland, College Park, MD 20742 USA

ABSTRACT

Computational micromagnetics plays an important role in design and control of magnetostrictive actuators. A systematic approach to calculate magnetic dynamics and magnetostriction is presented. A finite difference method is developed to solve the coupled Landau-Lifshitz-Gilbert (LLG) equation for dynamics of magnetization and a one dimensional elastic motion equation. The effective field in the LLG equation consists of the external field, the demagnetizing field, the exchange field, and the anisotropy field. A hierarchical algorithm using multipole approximation speeds up the evaluation of the demagnetizing field, reducing computational cost from $O(N^2)$ to $O(N \log N)$. A hybrid 3D/1D rod model is adopted to compute the magnetostriction: a 3D model is used in solving the LLG equation for the dynamics of magnetization; then assuming that the rod is along z -direction, we take all cells with same z -coordinate as a new cell. The values of the magnetization and the effective field of the new cell are obtained from averaging those of the original cells that the new cell contains. Each new cell is represented as a mass-spring in solving the motion equation. Numerical results include: 1. domain wall dynamics, including domain wall formation and motion; 2. effects of physical parameters, grid geometry, grid refinement and field step on $H - M$ hysteresis curves; 3. magnetostriction curve.

Keywords: Micromagnetics, magnetostrictive actuator, hysteresis

1. INTRODUCTION

Magnetostriction is the phenomenon of strong coupling between magnetic properties and mechanical properties of some ferromagnetic materials (e.g., Terfenol-D): strains are generated in response to an applied magnetic field, while conversely, mechanical stresses in the materials produce measurable changes in magnetization. This coupling has been used to design magnetostrictive actuators and sensors. Magnetostrictive actuators have numerous advantages, such as high energy density and capability of remote control.

The dynamic model of magnetostriction consists of two coupled parts: the magnetic part and the mechanical part. The magnetic part is governed by the Landau-Lifshitz-Gilbert (LLG) equation, a key equation in *micromagnetics*, while the mechanical part is governed by an elastic motion equation. Analytic solutions to these equations can be obtained only for a few simple cases. Thus numerical computation plays an important role in solving magnetoelasticity problems.

We present a systematic approach to calculate magnetic dynamics and magnetostriction in this paper. A hybrid 3D/1D rod model is adopted in the computation. Computational micromagnetics is of great interest in its own right¹⁻¹¹ and it has been widely used in the study of magnetic recording. The first part of our work is to solve the three dimensional micromagnetic problem using a finite difference method. Evaluation of the demagnetizing field is the most computation intensive part in any micromagnetic program. We have developed a fast hierarchical algorithm to accelerate the computation. In the second part, after we obtain the magnetization, we solve the one dimensional elastic motion equation to get the magnetostriction.

The paper is organized as follows. Continuous micromagnetics is introduced in Section 2 and its discretized version is described in Section 3. Computation method of magnetostriction is given in Section 4. Several implementation issues are discussed in Section 5. Numerical results are presented in Section 6, including domain wall dynamics, effects of parameters on $H - M$ hysteresis curves, and an example of magnetostriction curve. Section 7 provides concluding remarks.

* This research was supported by the Army Research Office under the ODDR&E MURI97 Program Grant No. DAAG55-97-1-0114 to the Center for Dynamics and Control of Smart Structures (through Harvard University).

Further author information: (Send correspondence to X.T.)

E-mail: X.T.: xbtan@isr.umd.edu J.S.B.: baras@isr.umd.edu P.S.K.: krishna@isr.umd.edu

2. CONTINUOUS FORMULATION OF MICROMAGNETICS

A ferromagnetic material is characterized by a spontaneous magnetization \mathbf{M} below the Curie temperature. The magnitude of \mathbf{M} , denoted as M_s , is uniform throughout a homogeneous specimen under the assumption of uniform temperature. The direction of \mathbf{M} , however, varies from one region to another, in the absence of an applied field, on a scale corresponding to visual observations with a microscope. A region with uniform \mathbf{M} is called a domain. The transitional region between domains is called a domain wall. Micromagnetics is a ferromagnetic theory which studies ferromagnetic materials on a scale that is small enough to reveal details of domain walls, yet much larger than the atomic scale.¹²

The free energy E of a ferromagnetic body is composed of several energy contributions; accordingly, several field contributions add up to the effective magnetic field \mathbf{H}_{eff} . An equilibrium configuration of \mathbf{M} can be found by locally minimizing the free energy. The Landau-Lifshitz-Gilbert (LLG) equation governs the dynamics of \mathbf{M} . Solving the LLG equation provides the dynamical evolution of \mathbf{M} as well as the equilibrium configuration of \mathbf{M} .

2.1. The Free Energy of a Ferromagnetic Material

The free energy of a ferromagnetic specimen can be written as a sum of several energy contributions,

$$E = E_{\text{ext}} + E_{\text{exch}} + E_{\text{anis}} + E_{\text{demag}}, \quad (1)$$

where E_{ext} is the energy due to the interaction between an applied field and magnetic moments, E_{exch} is the energy due to quantum-mechanical exchange effect between nearest neighbours, E_{anis} is the energy due to the crystalline anisotropy, and E_{demag} is the demagnetizing energy arising from the interactions of magnetic moments. Other energy terms may be included, such as the surface anisotropy energy and the magnetostrictive energy, but they are not considered here.

We can further express the individual energy terms. The CGS unit system is adopted in this paper. Assuming that the specimen occupies a region V ,

$$E_{\text{ext}} = - \int_V \mathbf{M} \cdot \mathbf{H}_{\text{ext}} d\tau, \quad (2)$$

$$E_{\text{exch}} = \int_V \frac{A_x}{M_s^2} (\|\nabla M_x\|^2 + \|\nabla M_y\|^2 + \|\nabla M_z\|^2) d\tau, \quad (3)$$

$$E_{\text{anis}} = \int_V K_u \left(1 - \left(\frac{M_z}{M_s}\right)^2\right) d\tau, \quad (4)$$

$$E_{\text{demag}} = -\frac{1}{2} \int_V \mathbf{M} \cdot \mathbf{H}_{\text{demag}} d\tau. \quad (5)$$

Here $d\tau$ is the volume element, \mathbf{M} is the vector magnetization, M_x, M_y, M_z are the x, y, z components of \mathbf{M} , M_s is the magnitude of \mathbf{M} , \mathbf{H}_{ext} is the externally applied field (which can be non-uniform), $\mathbf{H}_{\text{demag}}$ is the demagnetizing field (the expression of which is given later), A_x is the exchange stiffness constant, K_u is the anisotropy constant, “ ∇ ” represents the gradient, “ \cdot ” represents the inner product, and “ $\|\cdot\|$ ” represents the Euclidean norm of a 3D vector. Note that uniaxial anisotropy is assumed with z axis as the easy axis.

2.2. The Effective Field

The effective field \mathbf{H}_{eff} is defined via the variational derivative of E with respect to \mathbf{M} :

$$\mathbf{H}_{\text{eff}} = -\frac{\delta E}{\delta \mathbf{M}}. \quad (6)$$

Accordingly, we can write

$$\mathbf{H}_{\text{eff}} = \mathbf{H}_{\text{ext}} + \mathbf{H}_{\text{exch}} + \mathbf{H}_{\text{anis}} + \mathbf{H}_{\text{demag}}, \quad (7)$$

where \mathbf{H}_{ext} , \mathbf{H}_{exch} , \mathbf{H}_{anis} and $\mathbf{H}_{\text{demag}}$ are called external field, exchange field, anisotropy field, and demagnetizing field, respectively. The external field \mathbf{H}_{ext} is known to us in general, and \mathbf{H}_{exch} , \mathbf{H}_{anis} can be evaluated using formulae analogous to (6):

$$\mathbf{H}_{\text{exch}} = -\frac{\delta E_{\text{exch}}}{\delta \mathbf{M}} = \frac{2A_x \Delta \mathbf{M}}{M_s^2}, \quad (8)$$

$$\mathbf{H}_{\text{anis}} = -\frac{\delta E_{\text{anis}}}{\delta \mathbf{M}} = \left(0 \quad 0 \quad \frac{2K_u M_z}{M_s^2}\right)^T, \quad (9)$$

where “ Δ ” denotes the Laplacian and “ T ” represents matrix transpose. The demagnetizing field at \mathbf{r} , $\mathbf{H}_{\text{demag}}(\mathbf{r})$, can be written down directly from magnetostatics¹³:

$$\mathbf{H}_{\text{demag}}(\mathbf{r}) = -\int_V \frac{(\mathbf{r} - \mathbf{r}') \nabla \cdot \mathbf{M}(\mathbf{r}')}{\|\mathbf{r} - \mathbf{r}'\|^3} d\tau' + \oint_{\partial V} \frac{(\mathbf{r} - \mathbf{r}') \mathbf{M}(\mathbf{r}') \cdot \mathbf{n}(\mathbf{r}')}{\|\mathbf{r} - \mathbf{r}'\|^3} ds', \quad (10)$$

where $d\tau'$, ds' are the volume element and the area element, respectively, the integrals are taken over the space variable \mathbf{r}' , “ $\nabla \cdot$ ” is the divergence operator with respect to \mathbf{r}' , ∂V is the boundary of V , and $\mathbf{n}(\mathbf{r}')$ is the unit outward normal at \mathbf{r}' .

A first glance at (5) may lead to the doubt whether the “ $\frac{1}{2}$ ” is extra. It is not because each pairwise interaction of magnetic moments will appear in the demagnetizing energy expression twice. From (8)-(10), we see that \mathbf{H}_{exch} depends only on \mathbf{M} near the field point, \mathbf{H}_{anis} depends only on \mathbf{M} at the field point, while $\mathbf{H}_{\text{demag}}$ depends on the whole distribution of \mathbf{M} . This explains why the evaluation of the demagnetizing field is the most computation intensive part in micromagnetics.

2.3. The Landau-Lifshitz-Gilbert Equation

The governing equation of motion for \mathbf{M} is the Landau-Lifshitz-Gilbert (LLG) equation¹⁴:

$$\frac{\partial \mathbf{M}}{\partial t} = \gamma_0 \mathbf{M} \times \mathbf{H}_{\text{eff}} - \gamma_0 \eta \mathbf{M} \times \frac{\partial \mathbf{M}}{\partial t}, \quad (11)$$

where γ_0 is the gyromagnetic ratio (a negative constant), η is a positive constant, and “ \times ” denotes the vector product. The first term on the right hand side of (11) is a precessing term, which would rotate \mathbf{M} around \mathbf{H}_{eff} and maintain a fixed angle between them in the absence of the second term; the second term is a phenomenological damping term, which makes \mathbf{M} spiral towards \mathbf{H}_{eff} . Note that the condition for equilibria of LLG equation is $\mathbf{M} \times \mathbf{H}_{\text{eff}} = \mathbf{0}$, i.e., \mathbf{M} is parallel or antiparallel to \mathbf{H}_{eff} . Equation (11) can be manipulated into:

$$(1 + \alpha^2) \frac{\partial \mathbf{M}}{\partial t} = \gamma_0 \mathbf{M} \times \mathbf{H}_{\text{eff}} + \frac{\gamma_0 \alpha}{M_s} \mathbf{M} \times (\mathbf{M} \times \mathbf{H}_{\text{eff}}), \quad (12)$$

which is of the form of the original Landau-Lifshitz equation.¹⁵ Here $\alpha = |\gamma_0| \eta M_s$, and α is called the damping parameter. Equation (12) is the one we shall use in computation.

In the absence of surface anisotropy, at the boundary ∂V , we have¹²:

$$\mathbf{M} \times \frac{\partial \mathbf{M}}{\partial \mathbf{n}} = 0, \quad (13)$$

where $\frac{\partial \mathbf{M}}{\partial \mathbf{n}} \triangleq \nabla \mathbf{M} \cdot \mathbf{n}$. Since $\mathbf{M} \cdot \mathbf{M} = M_s^2$,

$$\mathbf{M} \cdot \frac{\partial \mathbf{M}}{\partial \mathbf{n}} = 0. \quad (14)$$

From (13) and (14), we obtain the boundary condition for (12):

$$\frac{\partial \mathbf{M}}{\partial \mathbf{n}} = 0. \quad (15)$$

3. DISCRETIZED FORMULATION OF MICROMAGNETICS

The geometry of a ferromagnetic body is assumed to be rectangular. We discretize the body into cells of size d_0 . The numbers of cells along the x, y, z axes are denoted by N_x, N_y and N_z . We assume that \mathbf{M} is constant within each cell. For the cell (i, j, k) , $1 \leq i \leq N_x, 1 \leq j \leq N_y, 1 \leq k \leq N_z$, $\mathbf{M}^{i,j,k}$ represents the magnetization of cell. Similar notations are used for the field terms. All the field terms are evaluated at the center of each cell.

As in Section 2,

$$\mathbf{H}_{\text{eff}}^{i,j,k} = \mathbf{H}_{\text{ext}}^{i,j,k} + \mathbf{H}_{\text{exch}}^{i,j,k} + \mathbf{H}_{\text{anis}}^{i,j,k} + \mathbf{H}_{\text{demag}}^{i,j,k}. \quad (16)$$

A 7-point stencil is adopted to approximate the 3D Laplacian in (8):

$$\mathbf{H}_{\text{exch}}^{i,j,k} = \frac{2A_x}{M_s^2 d_0^2} (\mathbf{M}^{i+1,j,k} + \mathbf{M}^{i-1,j,k} + \mathbf{M}^{i,j+1,k} + \mathbf{M}^{i,j-1,k} + \mathbf{M}^{i,j,k+1} + \mathbf{M}^{i,j,k-1} - 6\mathbf{M}^{i,j,k}). \quad (17)$$

The boundary condition (15) implies

$$\frac{\partial \mathbf{M}}{\partial x} = \frac{\partial \mathbf{M}}{\partial y} = \frac{\partial \mathbf{M}}{\partial z} = 0$$

at the boundary of the rectangular body in consideration. We enforce this condition by setting $\mathbf{M}^{N_x+1,j,k} = \mathbf{M}^{N_x,j,k}$, $\mathbf{M}^{0,j,k} = \mathbf{M}^{1,j,k}$, etc., when evaluating (17).

Discretization of (9) is straightforward:

$$\mathbf{H}_{\text{anis}}^{i,j,k} = \left(0 \quad 0 \quad \frac{2K_u M_z^{i,j,k}}{M_s^2} \right)^T. \quad (18)$$

$\mathbf{H}_{\text{demag}}^{i,j,k}$ is the sum of the demagnetizing field contributions at the center of cell (i, j, k) from all other cells. A fast hierarchical algorithm has been developed to evaluate the demagnetizing field, and it reduces computation cost from $O(N^2)$ to $O(N \log N)$.¹⁶

We now get a set of ordinary differential equation (ODE) from the LLG equation (12):

$$(1 + \alpha^2) \frac{d\mathbf{M}^{i,j,k}}{dt} = \gamma_0 \mathbf{M}^{i,j,k} \times \mathbf{H}_{\text{eff}}^{i,j,k} + \frac{\gamma_0 \alpha}{M_s} \mathbf{M}^{i,j,k} \times (\mathbf{M}^{i,j,k} \times \mathbf{H}_{\text{eff}}^{i,j,k}), \quad (19)$$

which will be integrated using the fourth order Runge-Kutta method to get the dynamics of $\mathbf{M}^{i,j,k}$. Note that we need to recompute $\mathbf{H}_{\text{eff}}^{i,j,k}$ after each iteration of all ODE's. The evolution of the total energy E can be monitored via

$$E = - \sum_{i,j,k} \mathbf{M}^{i,j,k} \cdot (\mathbf{H}_{\text{ext}}^{i,j,k} + \mathbf{H}_{\text{exch}}^{i,j,k} + \mathbf{H}_{\text{anis}}^{i,j,k} + \frac{1}{2} \mathbf{H}_{\text{demag}}^{i,j,k}) d_0^3. \quad (20)$$

4. COMPUTATION OF MAGNETOSTRICTION

We consider a rod-shaped magnetostrictive actuator. Mechanical dynamics of the rod is governed by the motion equation of continua:

$$\rho \dot{\mathbf{v}} = \rho \mathbf{M} \cdot \nabla \mathbf{H} + \nabla \cdot \mathbf{T}, \quad (21)$$

where ρ is the density, \mathbf{v} is the velocity, \mathbf{T} is the stress tensor. Since a 3D model is cumbersome in mechanical dynamics simulation, we use a 3D/1D hybrid model in calculation of magnetostriction. A 3D model is adopted in solving the LLG equation for dynamics of \mathbf{M} as done in Section 3; then assuming that the rod is along z axis, in consideration of the symmetry of the 3D model in $x - y$ plane, we take all $N_x N_y$ cells with same z -coordinate as a new cell. The values of \mathbf{M} and \mathbf{H}_{eff} of the new cell are obtained from averaging those of the original cells that it contains. In other words, the rod is now discretized into N_z cells in z direction only.

In the mechanical part simulation, each cell is represented by a mass-spring. Assume that the bottom surface of cell 1 is fixed while the top surface of cell N_z is free. The magnetic force plays the role of coupling the magnetic dynamics with the mechanical dynamics. Dynamics of each cell is governed by Newton's law. For cell i ($i = 1, \dots, N_z$), when motion is constrained in z direction,

$$m \dot{v}_z^i = F_{ez}^i + F_{mz}^i + F_{fz}^i, \quad (22)$$

where m is the mass of each cell, v_z^i is the velocity of cell i , $F_{ez}^i, F_{mz}^i, F_{fz}^i$ are z components of elastic force, magnetic force, and friction force acted on cell i , respectively. Each of the forces is further explained below.

Elastic force F_{ez}^i . Linearity of the springs is assumed, i.e.,

$$F_{ez}^i = k(d^{i+1} - d^i), \quad (23)$$

where k is the elastic constant of each spring, d^i is extension of spring i .

Magnetic force F_{mz}^i . The magnetic force $\mathbf{F}_m = \mathbf{M} \cdot \nabla \mathbf{H} vol$, where vol is the volume of each cell. Since we are only interested in the z component, $F_{mz} = (M_x \frac{\partial H_z}{\partial x} + M_y \frac{\partial H_z}{\partial y} + M_z \frac{\partial H_z}{\partial z}) vol$. Furthermore, 1D model leads to $\frac{\partial H_x}{\partial x} = \frac{\partial H_y}{\partial y} = 0$. Thus $F_{mz} = M_z \frac{\partial H_z}{\partial z} vol$. In computation, $\frac{\partial H_z}{\partial z}$ at cell i is approximated by

$$\frac{1}{2} \left(\frac{H_z^{i+1} - H_z^i}{z^{i+1} - z^i} + \frac{H_z^i - H_z^{i-1}}{z^i - z^{i-1}} \right),$$

where z^i denotes the position of cell i .

Note that since \mathbf{H} is discontinuous at the surface, we need to add a term F_{m0} to the top and bottom cells to account for the discontinuity,¹³ where

$$F_{m0} = 2K\pi M_z^2 vol.$$

For cell 1, $K = 0$ since the end of cell 1 is fixed; for cell N_z , $K = 1$.

Friction force F_{fz}^i . The friction force is used to speed up the process of approaching the mechanical equilibria. It is assumed that $F_{fz}^i = -\alpha_0 v_z^i$, where α_0 is the damping constant.

Assume that the original length of the magnetostrictive rod is l , then the magnetostriction is obtained by

$$\lambda = \frac{z^{N_z} - l}{l}, \quad (24)$$

where z^{N_z} is the position of the top cell at the equilibrium under some external field (with the assumption that the bottom position is 0).

5. IMPLEMENTATION ISSUES

An object-oriented 3D micromagnetics and magnetostriction computation program MM3 (MicroMagnetics in 3D) has been developed in C++. The data generated by MM3 are exported to Matlab for postprocessing.

We used

$$\frac{\| \mathbf{M}^{i,j,k} \times \mathbf{H}_{\text{eff}}^{i,j,k} \|}{\| \mathbf{M}^{i,j,k} \| \| \mathbf{H}_{\text{eff}}^{i,j,k} \|} \leq \epsilon, 1 \leq i \leq N_x, 1 \leq j \leq N_y, 1 \leq k \leq N_z,$$

as a criterion for equilibrium of magnetization. Here ϵ is a very small constant. Since the condition represents how well \mathbf{M} is parallel or antiparallel to \mathbf{H}_{eff} , it indicates how close the magnetization is to the equilibrium state. Note here the equilibria of a system of cells do not necessarily imply \mathbf{M} is parallel to \mathbf{H}_{eff} in every cell. In fact, it is often the case that \mathbf{M} is antiparallel to \mathbf{H}_{eff} in a few cells.

Variable step size was attempted but it didn't work well. One reason is that a too big step may not preserve the magnitude of magnetization and may also lead to the blowup of the algorithm due to the stiffness of the LLG equation, thus we have an upper bound on the step size. The other reason is that it is hard to find an appropriate criterion for varying step size. The energy was tried as a candidate, however, when the system approached the equilibrium, the energy was nearly constant (or even increasing) due to the precision of machines. This might lead the program into dead loops.

In the computation of magnetostriction, we first solve for the equilibria of magnetization, then solve for the mechanical equilibria. In other words, the magnetic and mechanical equations are not jointly solved. We treat the rod as a rigid body in computation of magnetization. The reason is that even for the so called "giant" magnetostrictive material, Terfenol-D, the highest magnetostriction is of order 10^{-3} . Thus ignoring the effect of deformation on magnetization will not introduce significant error but it greatly simplifies the computation.

6. NUMERICAL RESULTS

We have used the micromagnetic program to study domain wall dynamics, effects of various parameters on hysteresis curves and magnetostriction. $M_s = 1000emu$ is assumed in all computations.

6.1. Domain Wall Dynamics

Let $N_x = N_y = 1, N_z = 100$. This is essentially a 1D model.

6.1.1. Domain wall formation

Given some initial magnetization, under no external field, the magnetization will evolve to an equilibrium state, which is a local minimum of energy. We will see that in 1D case, magnetization in most cells will point in the z or $-z$ direction, and other cells constitute the transitional regions, i.e., domain walls.

Domain wall formation has been observed for two different initial conditions: linearly interpolated magnetization and randomly oriented magnetization. When no external field exists, linear initial magnetization results in one domain wall (Figure 1), while random initial magnetization results in multiple walls (Figure 2).

6.1.2. Domain wall motion

When a constant field is applied along z axis, domain wall forms and then moves out regardless of the magnitude of the external field (Figure 3). In this 1D model, we finally have a single domain oriented in the external field direction. This is due to the fact that the single domain structure has the minimum energy.¹² It also agrees with the result of the classical observations in experiment of Sixtus and Tonks.¹⁷

6.2. Effects of Parameters on $H - M$ Hysteresis Curves

The effects of various physical parameters, grid geometry, grid refinement, and field step on $H - M$ hysteresis loops are studied. H is the z component of the external field. M is the bulk magnetization along z axis:

$$M = \frac{\sum_{i,j,k} M_z^{i,j,k}}{N_x N_y N_z}.$$

When calculating the hysteresis loop, we assume that the external field is quasi-static, i.e., we let the external field be constant before the equilibrium is reached, then we increase (or decrease) the field by a fixed amount, i.e., the field step.

6.2.1. Effects of physical parameters

- **Anisotropy constant K_u .** From Figure 4, the bigger K_u is, the wider hysteresis loop is. This can be explained in the following way: when K_u is bigger, the anisotropy field becomes more important. Since it is always along the easy axis and agrees with z component of magnetization, it tries to prevent bulk magnetization from decreasing (in the sense of absolute value) too fast. On the other hand, stronger anisotropy makes approaching saturation faster.
- **Exchange constant A_x .** Figure 5 shows that when A_x gets bigger, the ferromagnetic material is harder; when A_x gets smaller, the demagnetizing field is more dominant and the Barkhausen effect becomes more evident.
- **Damping parameter α .** The precise value of the phenomenological damping parameter α is not known.³ People have found that the selected value for α does not markedly change the equilibrium profile, however, a larger value will lead to shorter computation time.³ This is true only when α is below some threshold value and it goes the other way when α is above the threshold, as shown in Figure 6.

6.2.2. Effect of grid geometry

From Figure 7, we can see that geometry plays a significant role in the shape of $H - M$ loop. Different sizes (with all other parameters same) leads to different shapes.

6.2.3. Effect of grid refinement

As shown in Figure 8, when the grid goes finer, the hysteresis loop does change with it; but the shape does not change significantly. This tells us that simulation on a coarse grid may still provide valuable information on the specimen. Since the dimensions of an actuator rod are often of order of several centimeters, the computation will be prohibitive if we divide the specimen into cells of very small size; however, from Figure 8, we are now more confident when using coarse grids.

6.3. Effect of field step

From Figure 9, we find that when the field step is too large, the hysteresis loop will distort drastically. Since the finer step implies more computation time, this is a problem of tradeoff.

6.4. Magnetostriction

Figure 10 gives an example of computed butterfly-shaped magnetostriction curve.

7. CONCLUSIONS

A framework for solving the coupled LLG equation and an elastodynamic equation has been presented. A 3D micromagnetic program is developed to calculate magnetization and magnetostriction for magnetostrictive actuators. The program may also be used in other general micromagnetic problems. It has been applied to the study of domain wall dynamics, $H - M$ hysteresis curves and magnetostriction curves. It can help understand behaviors of magnetostrictive materials. It can be used as a “numerical laboratory” to produce data for actuator modelling and design.

Current work includes developing a method for estimating mass-spring parameters from real material properties, and improving the magnetostriction model by including effects of bias field and prestress. Physical experiments will also be conducted to verify the numerical model.

REFERENCES

1. C. C. Shir, “Computations of the micromagnetic dynamics in domain walls,” *J. Appl. Phys.* **49**(6), pp. 3413–3421, 1978.
2. J. L. Blue and M. R. Scheinfein, “Micromagnetic calculations of 180° surface domain-wall magnetization profiles with comparison to measurements,” *J. Appl. Phys.* **68**(12), pp. 6504–6506, 1990.
3. M. R. Scheinfein and J. L. Blue, “Micromagnetic calculations of 180° surface domain walls,” *J. Appl. Phys.* **69**(11), pp. 7740–7751, 1991.
4. M. R. Scheinfein, J. L. Blue, and M. Aeschlimann, “Micromagnetics of surface segregation regions in domains written in TbFeCo alloys,” *IEEE Trans. Magn.* **27**(6), pp. 5124–5126, 1991.
5. M. R. Scheinfein, J. Unguris, J. L. Blue, K. J. Coakley, D. T. Pierce, and R. J. Celotta, “Micromagnetics of domain walls at surface,” *Phys. Rev. B* **43**(4), pp. 3395–3342, 1991.
6. D. R. Fredkin, T. R. Koehler, J. F. Smyth, and S. Schultz, “Magnetization reversal in permalloy particles: micromagnetic computation,” *J. Appl. Phys.* **69**(8), pp. 5276–527, 1991.
7. T. R. Koehler and D. R. Fredkin, “Finite element methods for micromagnetics,” *IEEE Trans. Magn.* **28**(2), pp. 1239–1244, 1992.
8. W. Chen, D. R. Fredkin, and T. R. Koehler, “A new finite element method in micromagnetics,” *IEEE Trans. Magn.* **29**(3), pp. 2124–2128, 1993.
9. B. Yang and D. R. Fredkin, “Dynamical micromagnetics by the finite element method,” *IEEE Trans. Magn.* **34**(6), pp. 3842–3852, 1998.
10. D. V. Berkov, K. Ramstöck, and A. Hubert, “Solving micromagnetic problems: towards an optimal numerical method,” *Phys. Stat. Sol. (a)* **137**(1), pp. 207–225, 1993.
11. R. H. Victora, “Quantitative theory for hysteretic phenomena in CoNi magnetic thin films,” *Phys. Rev. Lett.* **58**(17), pp. 1788–1791, 1987.
12. W. F. Brown, Jr., *Micromagnetics*, John Wiley & Sons, New York, 1963.
13. W. F. Brown, Jr., *Magnetoelastic interactions*, Springer-Verlag, Berlin, New York, 1966.

14. T. L. Gilbert, "A Lagrangian formulation of the gyromagnetic equation of the magnetization field," *Phys. Rev.* **100**, p. 1243, 1955.
15. L. Landau and E. Lifshitz, "On the theory of the dispersion of magnetic permeability in ferromagnetic bodies," *Phys. Z. Soviet Un.* **8**, pp. 153–169, 1935.
16. X. Tan, J. S. Baras, and P. S. Krishnaprasad, "Fast evaluation of demagnetizing field in three dimensional micromagnetics using multipole approximation," *Proc. SPIE* **3984**, 2000.
17. T. H. O'Dell, *Ferromagnetodynamics: the dynamics of magnetic bubbles, domains and domain walls*, John Wiley & Sons, New York, 1981.

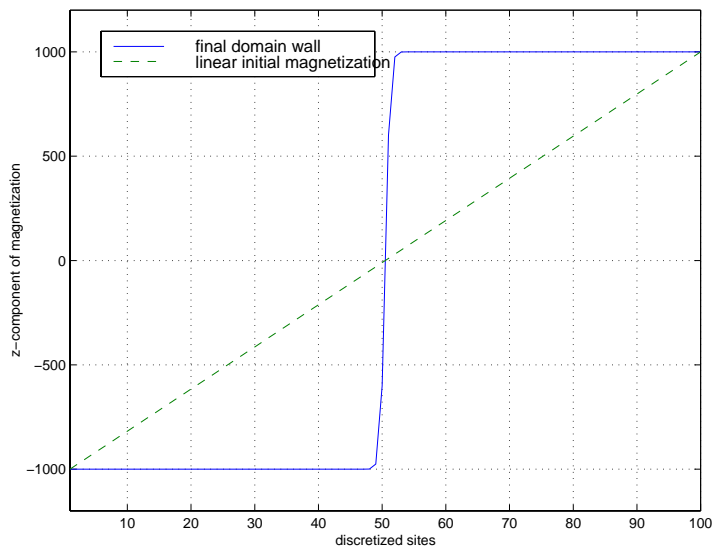


Figure 1. Domain wall formation with linear initialization (no external field).

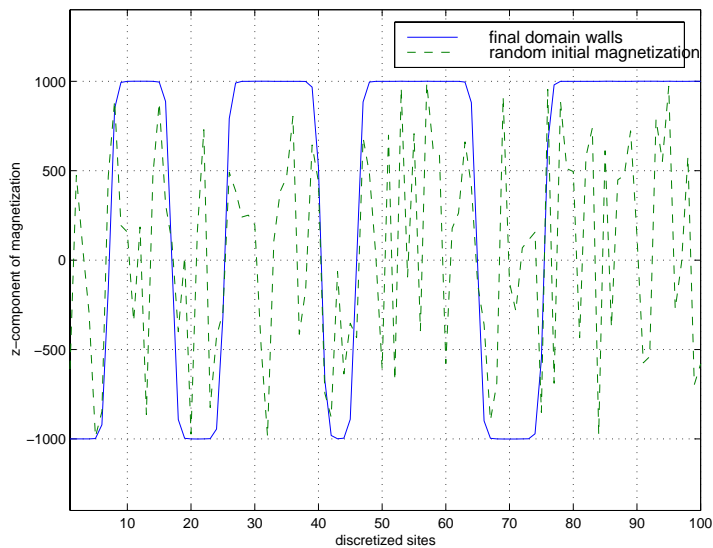


Figure 2. Domain wall formation with random initialization (no external field).

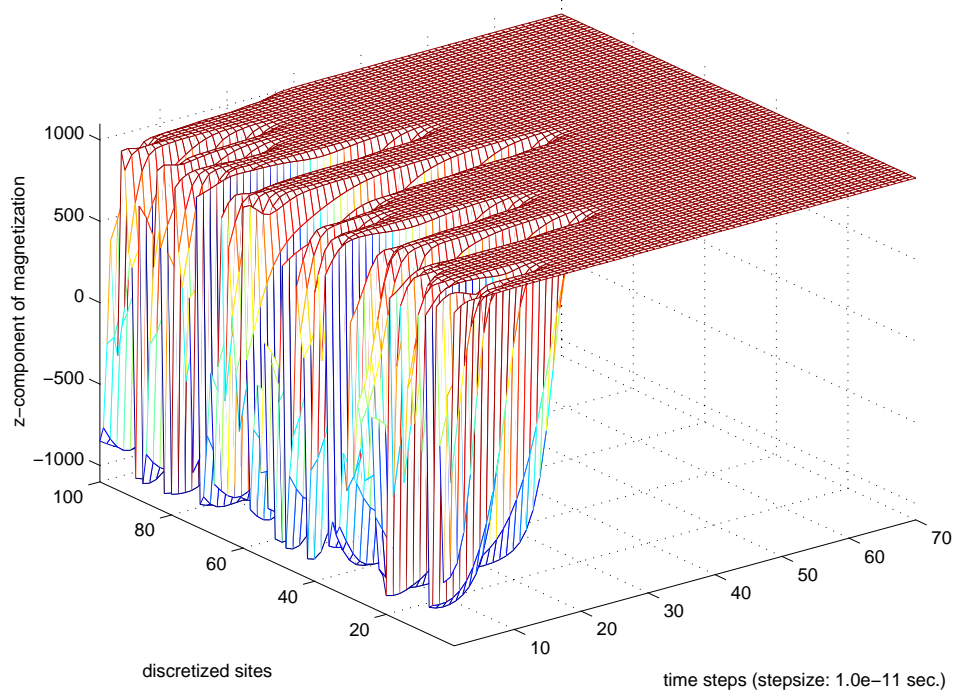


Figure 3. Domain walls move out under external field along z axis (random initialization).

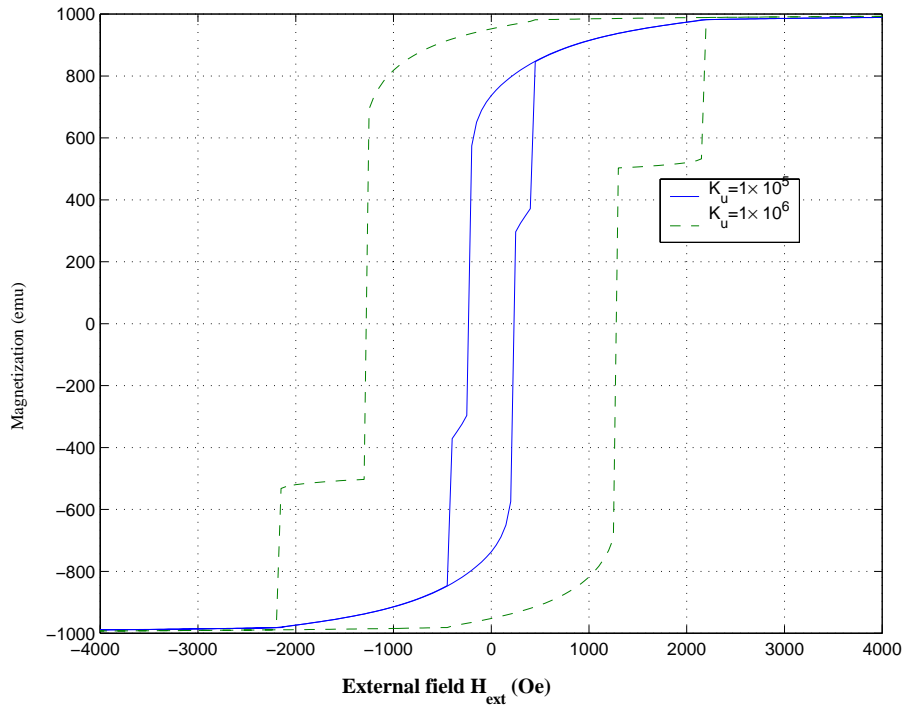


Figure 4. $H - M$ loops with different anisotropy constants K_u for a $4 \times 4 \times 8$ grid, cell size 10^{-6} cm , $A_x = 5 \times 10^{-7} \text{ erg/cm}$.

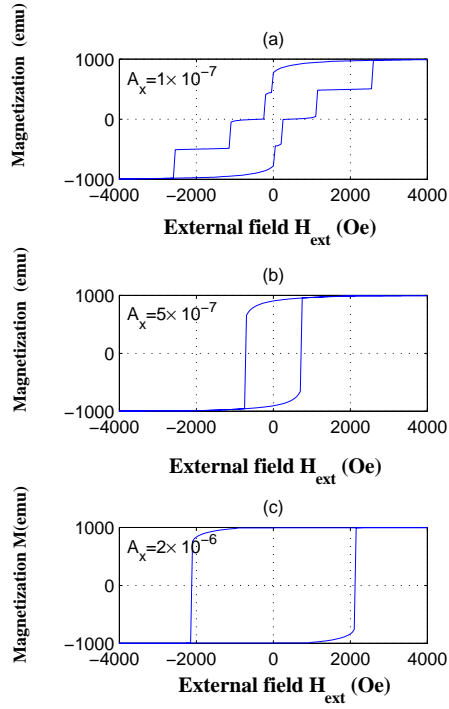


Figure 5. $H-M$ loops with different exchange constants A_x for a $4 \times 4 \times 16$ grid, cell size 10^{-6}cm , $K_u = 10^5 \text{erg/cm}^3$.

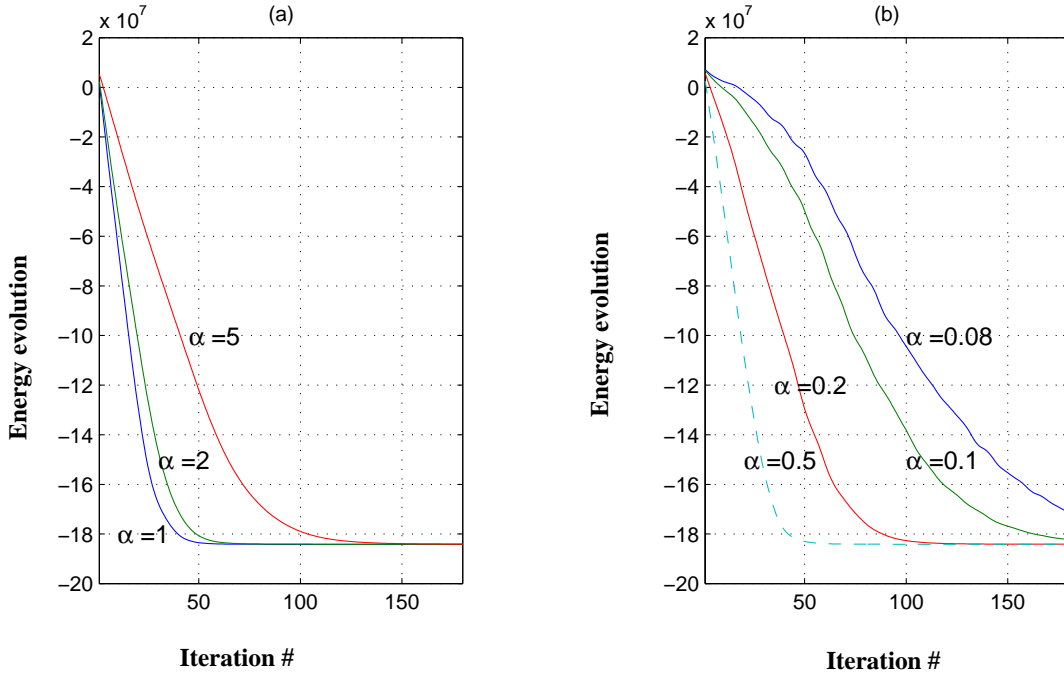


Figure 6. Energy evolution from linear initial magnetization to the equilibrium state under external field $h_{ext} = 4000 \text{Oe}$. In (a), damping constant α varies from 1 to 5; in (b), α varies from 0.08 to 0.5. Other parameters: $2 \times 2 \times 8$ grid, $K_u = 10^5 \text{erg/cm}^3$, cell size 10^{-6}cm , $A_x = 2 \times 10^{-7} \text{erg/cm}$.

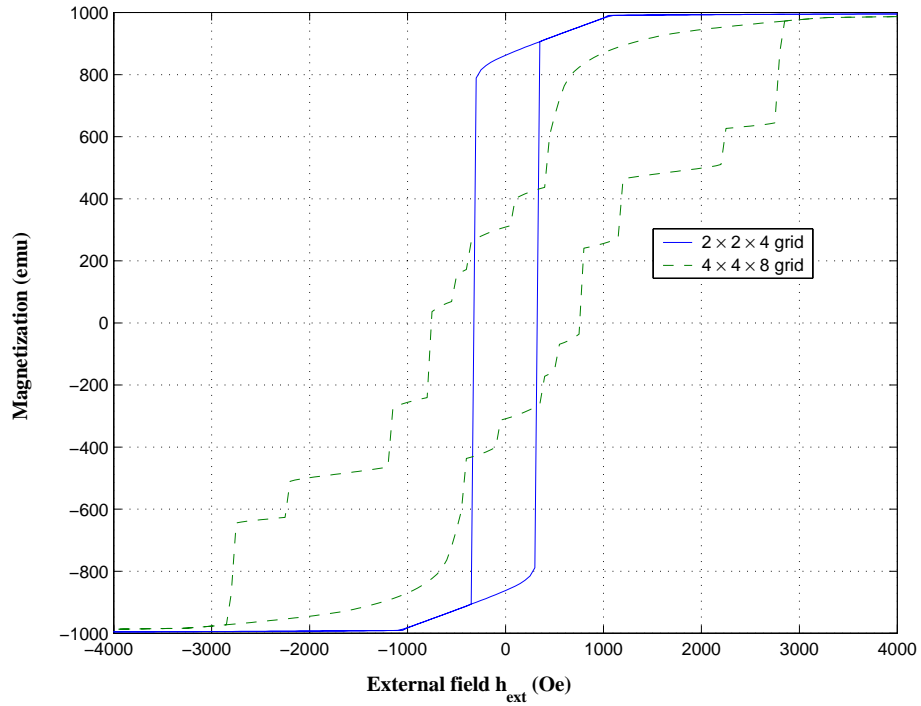


Figure 7. $H - M$ loops for different grids, cell size $10^{-6}cm$, $A_x = 2 \times 10^{-7}erg/cm$, $K_u = 10^5erg/cm^3$.

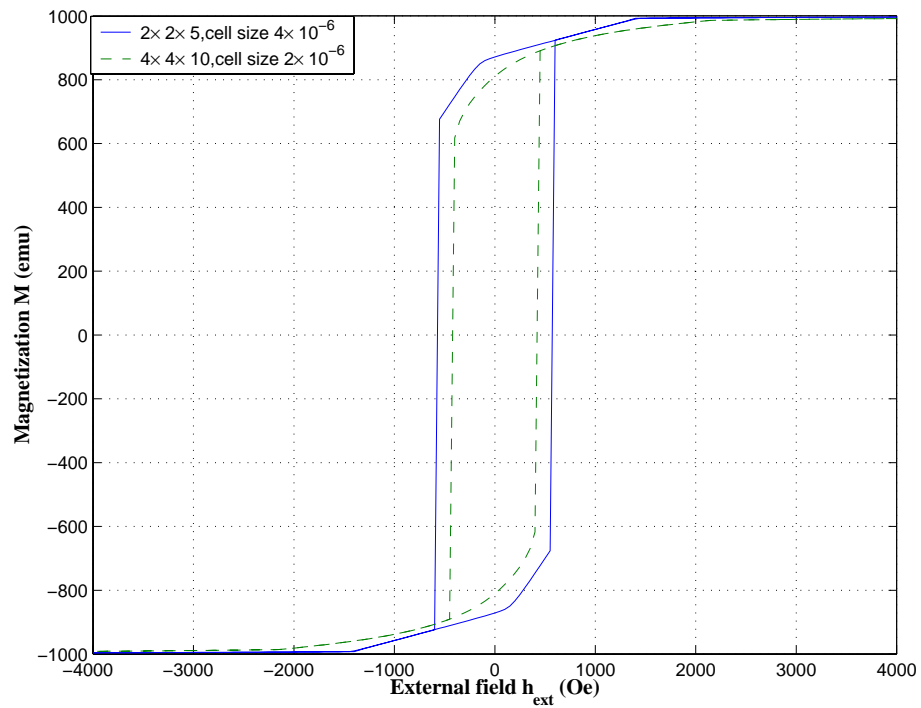


Figure 8. $H - M$ loops for different refinements, $A_x = 2 \times 10^{-6}erg/cm$, $K_u = 10^5erg/cm^3$.

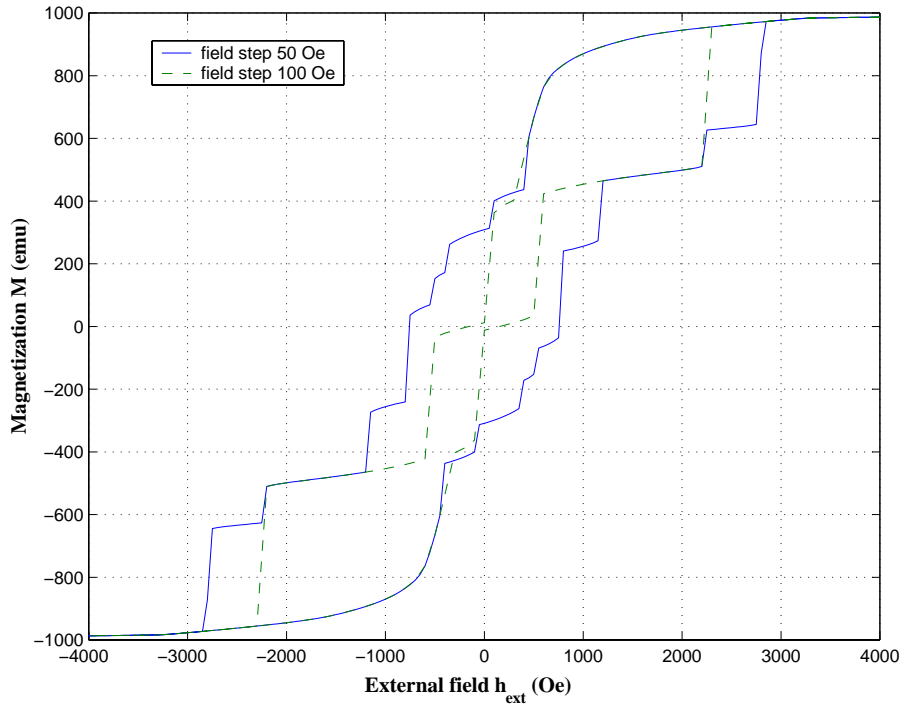


Figure 9. $H - M$ loops obtained using different field steps for a $4 \times 4 \times 8$ grid, $A_x = 2 \times 10^{-7} \text{erg/cm}$, $K_u = 10^5 \text{erg/cm}^3$.

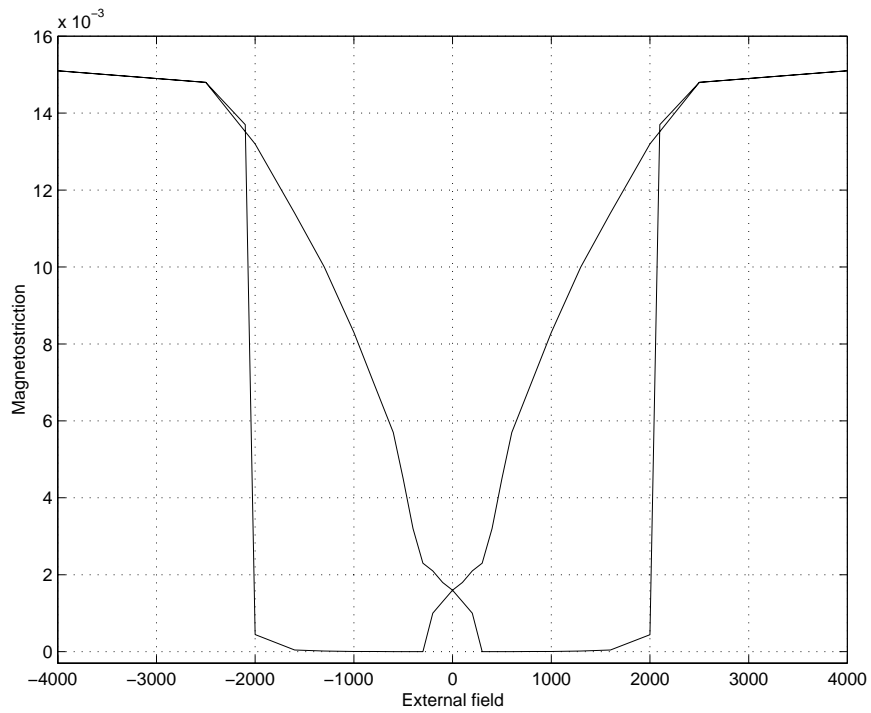


Figure 10. Magnetostriction curve. No bias field and no prestress.